# Effect of Model Resolution on Tropical Cyclone Climate Projections

Hiroyuki Murakami[1*] and Masato Sugi[2]

[1]*Advanced Earth Science and Technology Organization*, *Tokyo*, *Japan*
[2]*Research Institute for Global Change*, *JAMSTEC*, *Yokohama*, *Japan*

## Abstract

The effect of model resolution on projected climatological features of tropical cyclones (TCs) was investigated via 25-year present-day and future global warming projections using the Japan Meteorological Agency/Meteorological Research Institute Atmospheric General Circulation Model with four resolutions ranging from TL95 (180-km mesh) to TL959 (20-km mesh). The finest resolution (TL959) showed the highest skills in terms of TC intensity and interannual and seasonal variations in TC genesis number. Resolutions of TL319 (60-km mesh) and finer showed a significant future increase in the frequency of intense TCs, whereas resolutions coarser than TL319 showed no such change, indicating that TL319 is the critical resolution in projecting future change in the frequency of intense TCs. Overall, high model resolution is preferable for realistic and reliable climate projections. Resolutions of TL159 (120-km mesh) and finer showed similar skills, biases, and future changes in the spatial pattern of TC genesis frequency (TGF) and TC genesis number, indicating the potential use of lower model resolutions for minimizing uncertainties in future changes in the mean state of TGF and TC genesis number.

## 1. Introduction

While previous studies have conducted climate projections using state-of-the-art models (Knutson et al. 2010), one issue that has yet to be clearly addressed is the effect of model resolution on the climatological features of projected TCs. This lack of information reflects the fact that high-resolution global model projections remain extremely expensive; consequently, most climate runs are performed with a relatively coarse resolution (e.g., 100−200-km mesh). Bengtsson et al. (2007) investigated the differences in outputs between T63 (180-km mesh) and T213 (60-km mesh) resolutions, reporting that while the two resolutions are similar in terms of future changes in the spatial patterns of TC genesis frequency (TGF), they are critically different in terms of future changes in the frequency of intense TCs. However, a comparison based on only two resolutions appears to be insufficient to conclude the existence of resolution dependency.

Recent advances in computational resources have enabled climate projections using high-resolution atmospheric general circulation models (AGCMs) such as TL959 (triangular truncation 959 with a linear Gaussian grid, equivalent to a 20-km mesh horizontally), as reported by Oouchi et al. (2006; hereafter referred to as 'O06'). The present study investigates resolution-related differences in the projected features of TC climatology (e.g., TC intensity, temporal variations in TC genesis number, and the spatial pattern of TGF) using four resolutions, ranging from TL95 (180-km mesh) to TL959 (20-km mesh). The remainder of the manuscript is organized as follows. Section 2 presents model descriptions and methodology, Section 3 provides the results, and Section 4 summarizes the main conclusions.

Corresponding author: Hiroyuki Murakami, Meteorological Research Instutite (MRI), 1-1, Nagamine, Tsukuba, Japan. E-mail: himuraka@mri-jma.go.jp
*Present affiliation: Japan Agency for Marine-Earth Science and Technology (JAMSTEC), Japan.


## 2. Methodology

***2.1 Models, reanalysis, and best-track data***

Table 1 lists the models considered in this study. Models (a)−(d) are the Japan Meteorological Agency/Meteorological Research Institute AGCMs (JMA/MRI AGCM), one of which is the same model as that used in O06, but with model resolutions of (a) TL959 (20-km mesh), (b) TL319 (60-km mesh), (c) TL159 (120-km mesh), and (d) TL95 (180-km mesh). Description of the model and experimental settings are explained in Supplement 1 for details. The only difference among the models considered in this study is resolution except for TL959; i.e., TL959 contains both effect of high resolution and some parameter turnings. Verifications of present-day projections regarding some basic states are also described in Supplement 1 for each resolution.

Each resolution was employed for a pair of integrations: a present-day projection (1979−2003) with prescribed observed sea surface temperature (SST) and a global-warming projection (2075−2099) with prescribed future SST based on an ensemble mean of 18 IPCC-AR4 (Intergovernmental Panel for Climate Change Fourth Assessment Report, IPCC 2007) models projected under the IPCC Special Report on Emission Scenarios (SRES) A1B. The projections performed in this study are expected to be more reliable than those reported by O06 because we employ more realistic features in the experimental design (Supplement 1). For example, the future projection is prescribed by an 18-model ensemble mean of future SST change, whereas O06 used SST projected by a single model; in addition, the model simulations cover a 25-year period and include interannual variations in the SST forcing field, whereas O06 covered 10-year periods using climatological mean SST. Murakami et al. (2008) presented case studies of medium-range forecasts and reported that TL959 is more realistic than TL319 in terms of simulating TC intensity and development tendency. However, because the authors used initial conditions that contained existing TC structures, there remains uncertainty regarding the degree to which high resolution plays an important role in climate projections in which TCs are generated from scratch.

The Japanese Re-Analysis data (JRA-25; Onogi et al. 2007) were used for a test case employing the TC direct detection method described in Section 2.2. One of the advantages of JRA-25 is that it adopted TC retrieved (TCR) data in the assimilation process, leading to reasonable distributions of TC-like vorticities in the dataset (Hatsushika et al. 2006).

Observed TC "best-track" data were obtained from the Web site of Unisys Corporation (available online at http://weather.unisys.com/hurricane/), provided by the US Navy's Joint Typhoon

Table 1. Main features of the models considered in this study, including the threshold value of the relative vorticity criterion ($\zeta_{850}$) and the Taylor skill score I of tropical cyclone genesis frequency (TGF) against best-track data.

| Model/ Reanalysis name | Abbrevi-ation | Resolution (km) | $\zeta_{850}$ ($\times 10^{-5}$ s$^{-1}$) | Taylor skill score I |
|---|---|---|---|---|
| (a) JMA/MRI 20 km | TL959 | 20 × 20 | 31.28 | 0.87 |
| (b) JMA/MRI 60 km | TL319 | 60 × 60 | 11.43 | 0.82 |
| (c) JMA/MRI 120 km | TL159 | 120 × 120 | 8.33 | 0.87 |
| (d) JMA/MRI 180 km | TL95 | 180 × 180 | 7.68 | 0.80 |
| (e) Japanese Re-Analysis | JRA-25 | 140 × 140 | 0.62 | 0.96 |

Warming Center (JTWC) and by the National Hurricane Center (NHC) of the National Oceanographic and Atmospheric Administration, USA. In the present study, we only selected TCs with tropical storm intensity or stronger (i.e., those TCs that possess 1-minute sustained surface wind of 35 knots or greater).

### *2.2 TC detection method and definition of TGF*

Model-generated TCs were detected directly using globally uniform criteria similar to those reported in O06 (see Supplement 2 for details). In short, we incorporated five criteria: relative vorticity at 850 hPa ($\zeta_{850}$), dependent on model resolution (Table 1); temperature anomaly in the warm core region; maximum wind velocity at 850 hPa; genesis location; and duration. The resolution-dependent value of $\zeta_{850}$ ensures the observed global-mean annual TC number (i.e., 84.8 for the period 1979−2003) which is attained in the present-day simulation, for each resolution. The TC genesis locations were counted for each 5° × 5° grid area over the global domain. The total counts were defined as TGF in this study. Supplement 3 shows the TGF obtained from the best-track data, along with the result obtained by applying the above detection method to JRA-25 data. The detection method performs reasonably well in identifying observed TCs. The Taylor skill score I (i.e., the combination of the error and spatial correlation; Taylor 2001) for evaluating the spatial distributions of TGF shows a high value of 0.96 (Table 1).

The robustness of the present results, regardless of the defined grid box size, was experimentally confirmed using different grid box sizes (e.g., 2.5° × 2.5° or 10° × 10°; data not shown). We also experimentally applied a TC detection method using the objective resolution-dependent criteria proposed by Walsh et al. (2007), resulting in robust conclusions (data not shown). Nine ocean basins were considered for verifications: global (GL), Northern Hemisphere (NH), Southern Hemisphere (SH), North Indian Ocean (NIO), Western North Pacific (WNP), Eastern North Pacific (ENP), North Atlantic (NAT), South Indian Ocean (SIO), and South Pacific Ocean (SPO) (see Supplement 3 for region boundaries).

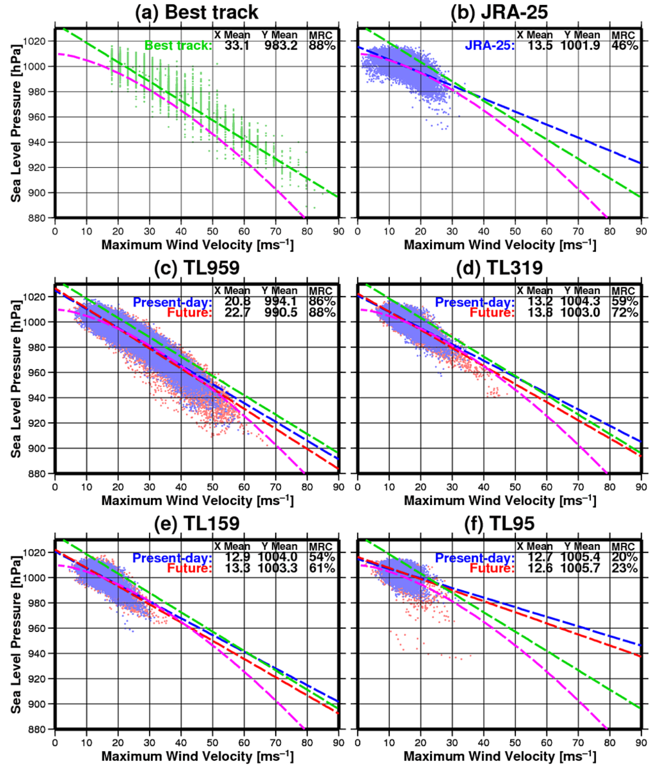


Fig. 1. Maximum wind velocity (MWV, unit: m s$^{-1}$) versus sea level pressure (SLP, unit: hPa) for (a) best-track data, (b) JRA-25, (c) TL959, (d) TL319, (e) TL159, and (f) TL95. The green, blue, and red lines are linear regression lines for the best track, present-day, and future projection data, respectively. The pink curve is the observed regression line proposed by Atkinson and Holiday (1977). Also listed in each panel are the values of mean MWS, SLP, and the multiple regression coefficient (MRC).

## 3. Results and discussion

### *3.1 Effect of model resolution on projected TC intensity*

Figure 1 shows the relationship between maximum wind velocity (MWV) and sea level pressure (SLP) for all detected TCs. Overall, TC intensity shows a dependency on horizontal resolution, although all resolutions more or less reproduce the observed relationship. Because JRA-25 (Fig. 1b) uses TL159 as the resolution in its assimilation process, the MWV−SLP relationship is similar to that obtained by TL159 (Fig. 1e). The regression lines for all resolutions are located below the green dashed regression line obtained for the best-track data. This discrepancy is mainly due to the differences in the definition of MWS; i.e., the best-track applies 1-minute sustained MWS, whereas the model applies time-step mean MWS (e.g., 10 min for TL959). However, the modeled relationships appear to be in good agreement with the observed regression line proposed by Atkinson and Holiday (1977; pink curves in Fig. 1). It is also evident that TL959 performs best in reproducing the observed intense TCs, although it still underestimates extremely intense TCs, such as those with MWV > 60 m s$^{-1}$ and SLP < 920 hPa.

For the future projections, all resolutions except for TL95 show an increase in mean TC intensity. However, in terms of the probability density of life-cycle maximum surface wind speed (Fig. 2), resolutions of TL319 and finer show a significant increase in the range of intense TCs, whereas resolutions of TL159 and coarser show no such significant increase. Previous studies that used a global model with a horizontal resolution of T106 (roughly equivalent to TL159 in the present study) reported no coherent changes in intense TCs in global warming experiments (Bengtsson et al. 1996; Sugi et al. 2002; Yoshimura et al. 2006; Gualdi et al. 2008). Moreover, Bengtsson et al. (2007) compared a global model with resolutions of T63 (192 × 96 grid) and T213 (640 × 320 grid), which are roughly equivalent to TL95 and TL319 in the present study, respectively. The authors reported that T213 showed a future increase in the frequency of intense TCs, whereas T63 did not. The authors also performed an additional experiment using a T319 (about 40-km mesh) model, which showed a clear increase in intense TCs in the future projection. Zhao et al. (2009) reported a significant increase in relatively intense TCs using a global model with 60-km grid spacing, which is equivalent to TL319 in the present study. Overall, 60-km mesh may be a critical resolution in projecting future increases in intense TCs. The view is supported by a recent report by Knutson et al. (2010). However, other factors (e.g., model physics) may also be relevant in this regard. Given that we are currently unable to explain why a 60-km mesh is a critical resolution, additional investigations are required.

### *3.2 Effect of resolution on projected TC genesis number*

Table 2 shows the percentage of model biases in annual mean TC genesis number for different basins. It must be noted that the basin-scale TC number is more or less independent of model resolution; e.g., all resolutions commonly underestimate TC numbers in NH, WNP and NAT, and overestimate TC numbers in SH, ENP, and SIO. Overall, it appears that the inter-basin balance in TC genesis number is not determined by the resolution, but by other parameters such as model physics. However, a comparison of inter-annual variations with observations reveals that finer resolutions show relatively higher skills (Table 3); e.g., TL959 shows statistically high correlation coefficients for four of the basins. The resolution dependency is clearer in the case of seasonal variations (Table 4).

Table 5 lists the percentage change in annual mean TC genesis number compared with the present-day projection. All resolutions except for TL95 share similarities in future changes; e.g., significant reductions in GL, NH, SH, WNP, ENP, SIO, and SPO, and

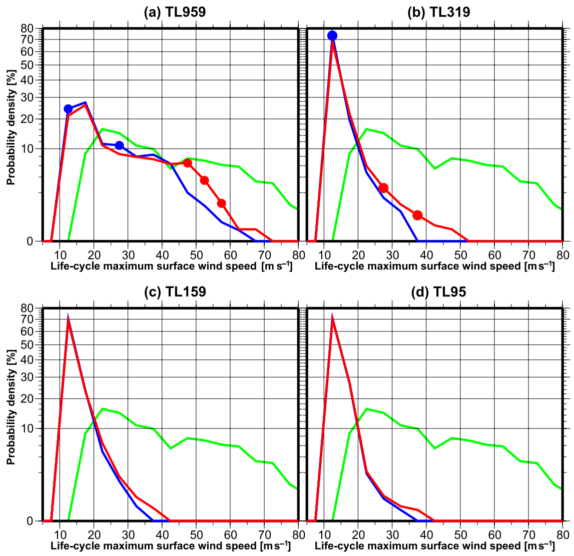


Fig. 2. Probability density of life-cycle maximum surface wind speed [m s$^{-1}$] for the global domain for observations (1979−2003, green lines), present-day projections (1979−2003, blue lines), and future projections (2075−2099, red lines) for resolutions of (a) TL959, (b) TL319, (c) TL159, and (d) TL95. The red (blue) circles indicate that the probability bin for the future projection is significantly higher (lower) than that for the present-day projection at the 95% level of significance (two-sided Student's *t*-test). Bin widths are 5 m s$^{-1}$.

Table. 2 Model biases in annual mean TC genesis number for each basin. The unit is percentage change compared with observations. Blue (red) numbers indicate that the negative (positive) bias is statistically significant at the 95% level (two-sided Student's *t*-test).

| | GL | NH | SH | NIO | WNP | ENP | NAT | SIO | SPO |
|---|---|---|---|---|---|---|---|---|---|
| TL959 | 0.0 | −10.0 | 22.5 | −10.5 | −40.5 | 55.2 | −38.4 | 20.4 | 20.9 |
| TL319 | 0.0 | −2.9 | 6.3 | 12.3 | −57.4 | 104.7 | −45.6 | 7.5 | −0.8 |
| TL159 | 0.0 | −5.9 | 13.3 | 23.7 | −47.4 | 69.2 | −35.7 | 12.3 | 11.0 |
| TL95 | 0.0 | −15.9 | 35.7 | 27.2 | −35.8 | 32.9 | −63.1 | 4.8 | 73.6 |

Table 3. Correlation coefficients for the inter-annual TC genesis number for each basin compared with observations. Red numbers indicate that the positive correlation coefficient is statistically significant at the 95% level (significance test for Pearson's product-moment correlation).

| | GL | NH | SH | NIO | WNP | ENP | NAT | SIO | SPO |
|---|---|---|---|---|---|---|---|---|---|
| TL959 | 0.28 | 0.11 | 0.53 | 0.14 | 0.60 | −0.33 | 0.42 | 0.48 | 0.17 |
| TL319 | 0.26 | 0.21 | 0.04 | 0.06 | 0.58 | −0.22 | 0.56 | 0.18 | −0.06 |
| TL159 | 0.17 | 0.23 | 0.22 | −0.04 | 0.44 | −0.04 | 0.24 | 0.25 | −0.13 |
| TL95 | 0.31 | 0.36 | 0.30 | 0.03 | 0.33 | −0.07 | −0.01 | −0.10 | 0.10 |

Table 4. As for Table 3, but for seasonal TC genesis number.

| | GL | NH | SH | NIO | WNP | ENP | NAT | SIO | SPO |
|---|---|---|---|---|---|---|---|---|---|
| TL959 | 0.82 | 0.93 | 0.99 | 0.91 | 0.86 | 0.83 | 0.99 | 0.95 | 0.98 |
| TL319 | 0.69 | 0.87 | 0.98 | 0.89 | 0.91 | 0.54 | 0.99 | 0.96 | 0.96 |
| TL159 | 0.56 | 0.80 | 0.98 | 0.66 | 0.91 | 0.39 | 0.97 | 0.98 | 0.96 |
| TL95 | 0.16 | 0.20 | 0.82 | 0.35 | −0.11 | 0.07 | 0.83 | 0.44 | 0.87 |

Table 5. As for Table 2, but for future changes in TC genesis number compared with the present-day projection.

| | GL | NH | SH | NIO | WNP | ENP | NAT | SIO | SPO |
|---|---|---|---|---|---|---|---|---|---|
| TL959 | −15.8 | −15.5 | −16.4 | −11.8 | −26.8 | −14.5 | 5.6 | −4.8 | −34.9 |
| TL319 | −18.8 | −18.9 | −18.5 | 18.0 | −11.7 | −30.5 | 4.2 | −8.9 | −33.7 |
| TL159 | −29.0 | −21.5 | −43.0 | −2.8 | −26.0 | −24.7 | −14.2 | −32.7 | −62.8 |
| TL95 | −1.2 | 8.6 | −14.8 | 22.1 | −18.5 | 17.3 | 56.7 | −17.0 | −14.3 |

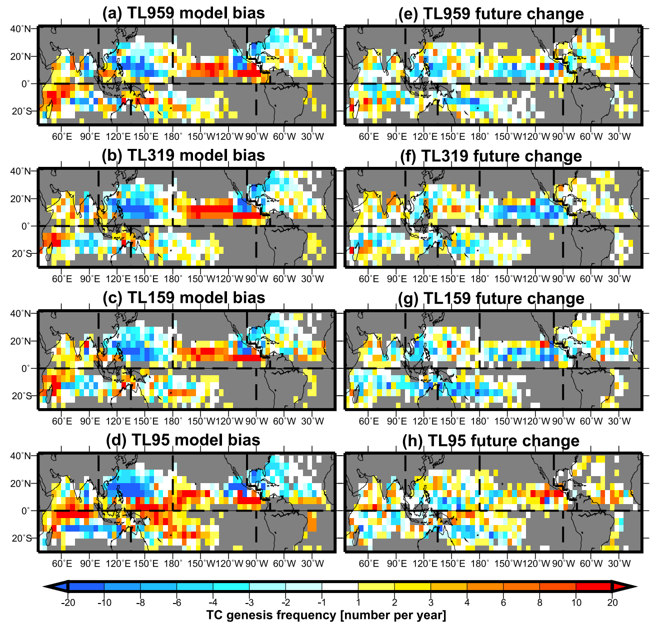


Fig. 3. (a−h) Biases and (e−h) future changes in tropical cyclone genesis frequency (TGF) projected by (a, e) TL959, (b, f) TL319, (c, g) TL159, and (d, h) TL95.

generally an increase in NAT. Although the relatively fine resolutions (TL959 and TL319) show similar future changes at hemispheric scales (GL, NH, and SH), they are inconsistent in several sub-basins in terms of both the sign and magnitude of change.

### *3.3 Effect of resolution on the projected spatial distributions of TC genesis frequency*

Figure 3a−d shows the spatial distributions of model biases in TGF for the present-day simulation for each resolution. All the resolutions show similarities in their biases: underestimates in the Bay of Bengal, WNP, coastal ENP, mid-latitudes of NAT, and central SIO, and overestimates in the Arabian Sea, South China Sea (SCS), central ENP, Inter-Tropical Convergence Zone (ITCZ) in NAT between 10°N and 20°N, African coastal SIO, and northeast Australia. When verified against observations, the Taylor skill score I (Table 1) shows similar values for the different resolutions. Table 6a lists the inter-resolution correlations for the spatial patterns of bias for the global domain, revealing correlation coefficients greater than 0.6, indicating that the model biases are common to the various resolutions.

Figure 3e−h shows similar future changes in TGF among the different resolutions, with general increases in TGF for the Arabian Sea, Bay of Bengal, southeastern quadrant of WNP, and the ITCZ in NAT; decreases are seen in SCS, central SIO, and northeast Australia. Table 6b indicates that each resolution, except

Table 6. (a) Inter-resolution correlation coefficients for biases of tropical cyclone genesis frequency (TGF). Red numbers indicate that the positive correlation coefficient is statistically significant at the 95% level (significance test for Pearson's product-moment correlation). (b) As for (a), but for future changes in TGF.

(a)

| | TL959 | TL319 | TL159 | TL95 |
|---|---|---|---|---|
| TL959 | | 0.80 | 0.74 | 0.63 |
| TL319 | | | 0.87 | 0.61 |
| TL159 | | | | 0.63 |
| TL95 | | | | |

(b)

| | TL959 | TL319 | TL159 | TL95 |
|---|---|---|---|---|
| TL959 | | 0.31 | 0.20 | 0.02 |
| TL319 | | | 0.37 | 0.00 |
| TL159 | | | | 0.11 |
| TL95 | | | | |

for TL95, shows a positive correlation with the other resolutions in terms of future change in TGF, although the correlation coefficients are smaller than those for bias (Table 6a). Moreover, similar resolutions show relatively strong correlations (e.g., TL959 and TL319, TL319 and TL159, and TL159 and TL95) compared with other resolution combinations, indicating that similar resolutions tend to show comparable spatial changes in TGF. Overall, future changes in TGF are independent of resolution; instead, they appear to be sensitive to model physics and the spatial pattern of prescribed SST (Sugi et al. 2009).

## 4. Conclusion

This study investigated the effect of model resolution on projected TC climatology, temporal variations in TC genesis, and future changes using four different resolutions, ranging from TL95 (180-km mesh) to TL959 (20-km mesh). The finest resolution (TL959) showed the highest skills in terms of mean TC intensity, and inter-annual and seasonal variations in TC genesis number, indicating that a high resolution is generally desirable for accurate projections of TC intensity and temporal variations in TC genesis. However, TL959 contains parameter tunings in the physical processes, indicating both effects of high-resolution and turning. Even if TL959 is removed from the comparisons, TL319 still shows the highest skills among coarser models, indicating high resolution is still preferable.

Regarding future changes in TC intensity, resolutions of TL319 (60-km mesh) and finer projected a significant future increase in the frequency of intense TCs; this significant increase was not projected by resolutions coarser than TL319. Comparisons with other studies that employed global models reveal that TL319 may be a critical resolution in terms of projecting future increases in the frequency of intense TCs.

Biases in basin-scale annual mean TC genesis number and the spatial distributions of TC genesis frequency (TGF) were not critically dependent on resolution, indicating the influence of other parameters such as model physics. Moreover, the nature of future changes is similar among the various resolutions, indicating that future changes in climatological mean features projected by a high-resolution model could also be obtained using coarser resolutions.

In summary, the use of a higher-resolution model is generally desirable for accurate climate projections, although in the present study, future changes and present-day climatology in TGF showed little dependence on resolution, except for TL95. This finding indicates the potential validity of using a model with relatively coarse resolution. For example, ensemble realizations may be useful in minimizing uncertainties in future projections that are difficult to perform with a higher-resolution model due to the large demand on computational resources. A model with coarse resolution may also be useful in a model-development process in improving the TGF climatology for better climate projections that would later be performed using a higher-resolution model. For future work, it is worthwhile investigating why there exists a critical resolution for projected future increases in the frequency of severe TCs.

## Acknowledgements

This work was conducted under the framework of the "Projection of the Change in Future Weather Extremes Using Super-High-Resolution Atmospheric Models" project supported by the KAKUSHIN program of the Ministry of Education, Culture, Sports, Science, and Technology (MEXT) of Japan.

The authors gratefully acknowledge the opportunity of this study provided by MRI.

## Supplements

Supplement 1 provides model description, a schematic diagram of the prescribed lower boundary conditions, and verifications of basic states for each resolution.

Supplement 2 describes the TC detection method.

Supplement 3 shows the TGF global distributions by JRA-25.

## References

Atkinson, G. D., and C. R. Holiday, 1977: Tropical cyclone minimum sea level pressure/maximum sustained wind relationship for the western North Pacific. *Mon. Wea. Rev.*, **105**, 421−427.

Bengtsson, L., M. Botzet, and M. Esch, 1996: Will greenhouse gas-induced warming over the next 50 years lead to higher frequency and greater intensity of hurricanes? *Tellus*, **48A**, 57−73.

Bengtsson, L., K. Hodges, M. Esch, N. Keenlyside, L. Kornblueh, J.-J. Luo, and T. Yamagata, 2007: How may tropical cyclones change in a warmer climate? *Tellus*, **59A**, 539−561.

Gualdi, S., E. Scoccimarro, and A. Navarra, 2008: Changes in tropical cyclone activity due to global warming: Results from a high-resolution coupled general circulation model. *J. Climate*, **21**, 5204−5228.

Hatsushika, H., J. Tsutsui, M. Fiorino, and K. Onogi, 2006: Impact of wind profile retrievals on the analysis of tropical cyclones in the JRA-25 reanalysis. *J. Meteor. Soc. Japan*, **5**, 891−905.

IPCC, 2007: *Climate change 2007: The physical science basis. Contribution of Working Group I to the Fourth Assessment Report of the Intergovernmental Panel on Climate Change*, Cambridge University Press, 996 pp.

Knutson, T. R., J. L. McBride, J. Chan, K. Emanuel, G. Holland, C. Landsea, I. Held, J. P. Kossin, A. K. Srivastava, and M. Sugi, 2010: Tropical cyclone and climate change, *Nat. Geosci.*, **3**, 157−163.

Murakami, H., T. Matsumura, R. Sakai, A. Noda, and S. Kusunoki, 2008: Verification typhoon forecasts for a 20km-mesh high-resolution global model. *J. Meteor. Soc. Japan*, **86**, 669−698.

Onogi, K., J. Tsutsui, H. Koide, M. Sakamoto, S. Kobayashi, H. Hatsushika, T. Matsumoto, N. Yamazaki, H. Kamahori, K. Takahashi, S. Kadokura, K. Wada, K. Kato, R. Oyama, T. Ose, N. Mannoji, and R. Taira, 2007: The JRA-25 reanalysis. *J. Meteor. Soc. Japan*, **85**, 369−432.

Oouchi, K., J. Yoshimura, H. Yoshimura, R. Mizuta, S. Kusunoki, and A. Noda, 2006: Tropical cyclone climatology in a global-warming climate as simulated in a 20km-mesh global atmospheric model: Frequency and wind intensity analysis. *J. Meteor. Soc. Japan*, **84**, 259−276.

Sugi, M., A. Noda, and N. Sato, 2002: Influence of the global warming on tropical cyclone climatology. *J. Meteor. Soc. Japan*, **80**, 249−272.

Sugi, M., H. Murakami, and J. Yoshimura, 2009: A reduction in global tropical cyclone frequency due to global warming. *SOLA*, **5**, 164−167.

Taylor, K. E., 2001: Summarizing multiple aspects of model performance in a singlediagram. *J. Geophys. Res.*, **106**, D7, 7183−7192.

Walsh, K. J. E., M. Fiorino, C. W. Landsea, and K. L. McInnes, 2010: Objectively determined resolution-dependent threshold criteria for the detection of tropical cyclones in climate models and reanalyses. *J. Climate*, **20**, 2307−2314.

Yoshimura, J., M. Sugi, and A. Noda, 2006: Influence of greenhouse warming on tropical cyclone frequency. *J. Meteor. Soc. Japan*, **84**, 405−428.

Zhao, M., I. M. Held, S.-J. Lin, and G. A. Vecchi, 2009: Simulations of global hurricane climatology, interannual variability, and response to global warming using a 50 km resolution GCM. *J. Climate*, **22**, 333−363.

*Manuscript received 19 February 2010, accepted 21 April 2010*
*SOLA: http://www.jstage.jst.go.jp/browse/sola/*